

Nonlinear Model Predictive Control of a High-Speed Linear Axis Driven by Pneumatic Muscles

Dominik Schindele and Harald Aschemann

Abstract—This paper presents a nonlinear predictive control scheme for a new linear axis. Its guided carriage is driven by a nonlinear mechanism consisting of a rocker with a pair of pneumatic muscle actuators arranged at both sides. This innovative drive concept allows for an increased workspace as well as higher carriage velocities as compared to a direct actuation. Modelling leads to a system of nonlinear differential equations including polynomial approximations of the volume characteristic as well as the force characteristic of the pneumatic muscles. For the control of the carriage position and the mean pressure a nonlinear model predictive trajectory control is designed. The main idea of the used method consists in a minimization of the tracking error at the end of the prediction horizon. That way the computation load can be kept relatively small. Remaining model uncertainties as well as nonlinear friction can be counteracted by an observer-based disturbance compensation. Experimental results from an implementation on a test rig show a high control performance.

I. INTRODUCTION

As shown in earlier work [1], [2] pneumatic muscles in combination with sophisticated nonlinear control can be used in motion control applications where precise tracking control of desired trajectories is required. Due to this fact, current research at the University of Rostock focusses on the use of pneumatic muscles as low-cost actuators in robotics. Pneumatic muscles are tension actuators consisting of a fiber-reinforced vulcanised rubber tubing with connection flanges at both ends. Because of a special fiber arrangement, the pneumatical muscle contracts with increasing internal pressure, which can be used for actuation purposes. Pneumatic muscles offer major advantages in comparison to classical pneumatic cylinders. They have significantly less weight, there are no stick-slip effects, the muscles are insensitive to dirty working environment and they have a larger maximum force. The nonlinear characteristics of the muscle, however, demand for nonlinear control, e.g. optimal control in earlier research [2]. There, a nonlinear control scheme for a one-degree-of-freedom linear axis directly driven by pneumatic muscles was presented. To increase both the available workspace and the maximum velocity of the carriage, a new nonlinear drive mechanism is employed as depicted in fig. 1. Here, two guideways with roller bearing units allow for rectilinear movements of the carriage with relatively small friction forces. The carriage is driven by a rocker. A bearing unit at the head of the rocker allows for both rotational and translational relative motion and transmits the drive force to the carriage. The rocker is actuated by a pair of pneumatic

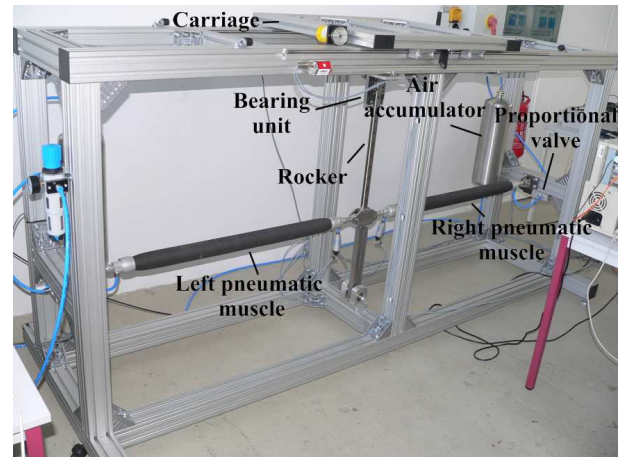


Fig. 1: High-speed linear axis

muscles in an antagonistic arrangement. The mounting points of the pneumatic muscles at the rocker have been defined so as to gain a reasonable trade-off between increase in maximum velocity and reduction of the achievable drive force. The mass flow rate of compressed air in and accordingly out of each pneumatic muscle is controlled by means of a separate proportional valve. The incoming air is available at a maximum pressure of 7 bar, whereas the outlet air is discharged at atmospheric pressure, i.e. 1 bar. Pressure declines in the case of large mass flow rates are avoided by using an air accumulator for each muscle.

The paper is structured as follows: first, the modelling of the mechatronic system is addressed. For the nonlinear characteristics of the pneumatic muscle, i.e. the muscle volume and the muscle force, polynomial descriptions are used in terms of contraction length and internal muscle pressure. Second, a nonlinear model predictive trajectory control scheme for the linear axis is proposed, which aims at reducing the predicted state error. For the control design the carriage position and the mean muscle pressure of the pair of pneumatic muscles serve as controlled variables. A disturbance force resulting from remaining modelling errors w.r.t. the force characteristic of the pneumatic muscles as well as the friction characteristic of the carriage is compensated by a nonlinear reduced-order disturbance observer. By this, desired trajectories for both carriage position and mean pressure can be tracked with high accuracy as shown by experimental results from an implementation at a test rig.

D. Schindele and H. Aschemann are with the Chair of Mechatronics, University of Rostock, Germany {dominik.schindele, harald.aschemann}@uni-rostock.de

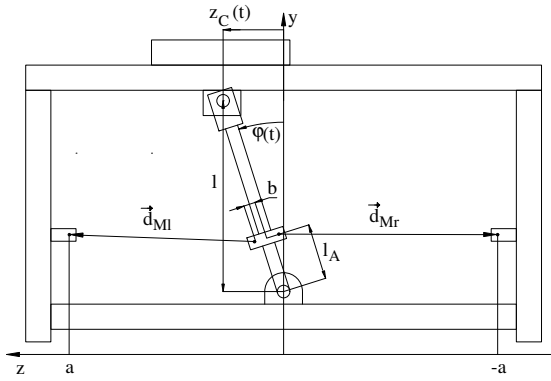


Fig. 2: Kinematical structure of the high-speed linear axis

II. MODELLING OF THE MECHATRONIC SYSTEM

As for modelling, the mechatronic system under consideration is divided in a mechanical and a pneumatic subsystem, which are coupled by the drive torque resulting from the tension forces of the pair of pneumatic muscles. In contrast to the model of [3] the dynamics of the pneumatic subsystem is taken into consideration as well.

A. Modelling of the mechanical subsystem

The chosen mechanical model for the high-speed linear axis consists of the following three elements (fig. 2): a rigid body for the rocker as actuated link (mass m_R , reduced mass moment of inertia w.r.t. the rocker joint J_R , distance s_R to the centre of gravity C_R , varying length of the link l_R), a single lumped mass for the lateral connecting rods (mass m_A , centre of gravity distance l_A to the rocker joint) and a lumped mass for the carriage (mass m_C).

The inertial yz -coordinate system is chosen in the base joint of the rocker. The mounting points of the pneumatic muscles at the rocker are characterised by the distance l_A in longitudinal direction and the perpendicular distance b of the lateral connecting rods as shown in fig. 2. The motion of the high-speed axis is completely described by the generalised coordinate $\varphi(t)$, which denotes the inclination of the rocker w.r.t. the plumb line. The carriage position is related to the rocker angle by the horizontal component $z_C(t) = l \cdot \tan \varphi(t)$, where l denotes the length between the mounts at the head and the bottom of the rocker at carriage position $z_C = 0$. The equation of motion directly follows from Lagrange's equations in form of a second order differential equation

$$J(\varphi)\ddot{\varphi} + k(\varphi, \dot{\varphi}) = \tau - \tau_U, \quad (1)$$

with the resulting mass moment of inertia $J(\varphi) = m_C \cdot l^2 \cdot (1 + \tan^2 \varphi)^2 + J_R + m_A \cdot l_A^2$ and the term $k(\varphi, \dot{\varphi}) = 2 \cdot m_C \cdot l^2 \cdot (1 + \tan^2 \varphi)^2 \cdot \tan \varphi \cdot \dot{\varphi}^2 - (m_R/2 \cdot l + m_A \cdot l_A) \cdot g \cdot \sin \varphi$, which takes into account the centrifugal as well as the gravity forces. The drive torque τ resulting from the muscle forces F_{Mi} , $i = \{l, r\}$ can be stated as

$$\tau = \vec{e}_x \cdot (F_{Mr} \cdot \vec{r}_{Fr} \times \vec{e}_{Mr} + F_{Ml} \cdot \vec{r}_{Fl} \times \vec{e}_{Ml}), \quad (2)$$

with the unity vector $\vec{e}_x = [1, 0, 0]^T$ in x -direction and the unity vectors $\vec{e}_{Mi} = \vec{d}_{Mi}/d_{Mi}$ in direction of the pneumatic muscle forces. The position vectors \vec{r}_{Fi} describe the connecting points, where the muscle forces act on the rocker. All remaining model uncertainties are taken into account by the disturbance torque τ_U . On the one hand, these uncertainties stem from approximation errors concerning the static muscle force characteristics and non-modelled viscoelastic effects of the vulcanised rubber material. On the other hand, time-varying damping and friction acting on the carriage as well as on the rocker depend in a complex manner on lots of influence factors and cannot be accurately represented by a simple friction model.

B. Modelling of the pneumatic subsystem

A mass flow \dot{m}_{Mi} , $i = \{l, r\}$ into the pneumatic muscle leads to an increase in internal pressure p_{Mi} , and a contraction $\Delta \ell_{Mi}$ of the muscle in longitudinal direction due to specially arranged fibers. The maximum contraction length $\Delta \ell_{M,max}$ is given by 25% of the uncontracted length. This contraction effect can be exploited to generate forces. The force F_{Mi} and the volume V_{Mi} of a pneumatic muscle depend nonlinear on the according internal pressure p_{Mi} and the contraction length $\Delta \ell_{Mi}$. The definition of the contraction length can be derived from fig. 2. Given the length of the uncontracted muscle ℓ_M , the contraction length of a pneumatic muscle can be calculated with the distance $d_{Mi} = |\vec{d}_{Mi}|$ between both connecting points of each muscle $i = \{l, r\}$. Simple geometrical considerations lead to the length of the left respectively right pneumatic muscle

$$d_{Mi} = \sqrt{d_{Miy}^2 + d_{Miz}^2}, \quad (3)$$

with $d_{Miy} = -\ell_A \cdot \cos \varphi \pm b \cdot \sin \varphi + \ell_A$ and $d_{Miz} = -\ell_A \cdot \sin \varphi \mp b \cdot \cos \varphi \pm a$. As a result, the contraction lengths for both pneumatic muscles are related to the rocker angle

$$\Delta \ell_{Mi} = \ell_M - d_{Mi}(\varphi). \quad (4)$$

The dynamics of the internal muscle pressure follows directly from a mass flow balance in combination with the energy equation for the compressed air in the muscle. As the internal muscle pressure is limited by a maximum value of $p_{Mi,max} = 7 \text{ bar}$, the ideal gas equation represents an accurate description of the thermodynamic behaviour. The thermodynamic process is modelled as a polytropic change of state with $n = 1.26$ as identified polytropic exponent. The identified volume characteristic (fig. 3) of the pneumatic muscle can be described by a polynomial function of both contraction length $\Delta \ell_{Mi}$ and the muscle pressure p_{Mi}

$$V_{Mi}(\Delta \ell_{Mi}, p_{Mi}) = \sum_{j=0}^3 a_j \cdot \Delta \ell_{Mi}^j \cdot \sum_{k=0}^1 b_k \cdot p_{Mi}^k. \quad (5)$$

The resulting state equation for the internal muscle pressure

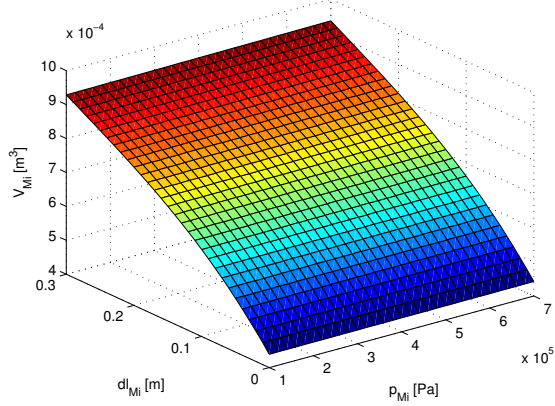


Fig. 3: Identified volume characteristic of the pneumatic muscle

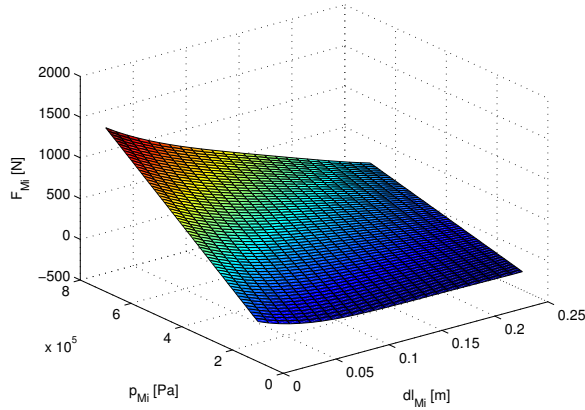


Fig. 4: Identified force characteristic of the pneumatic muscle

in the muscle i is given by

$$\dot{p}_{Mi} = \frac{n}{V_{Mi} + n \cdot \frac{\partial V_{Mi}}{\partial p_{Mi}} \cdot p_{Mi}} [u_{Mi} - \frac{\partial V_{Mi}}{\partial \Delta \ell_{Mi}} \cdot \frac{\partial \Delta \ell_{Mi}}{\partial \varphi} \cdot p_{Mi} \cdot \dot{\varphi}], \quad (6)$$

where $u_{Mi} = R_L \cdot T_{Mi} \cdot \dot{m}_{Mi}$ denotes the input variable. The internal temperature T_{Mi} can be approximated with good accuracy by the constant temperature T_0 of the ambience, see [4]. In this way, temperature measurements can be avoided, and the implementational effort is significantly reduced. The force characteristic $F_{Mi}(p_{Mi}, \Delta \ell_{Mi})$ of a pneumatic muscle states the resulting tension force for given internal pressure p_{Mi} as well as given contraction length $\Delta \ell_{Mi}$ and represents the connection of the mechanical and the pneumatic system part. The nonlinear force characteristic (fig. 4) has been identified by static measurements and, then, approximated by the following polynomial description

$$F_{Mi}(p_{Mi}, \Delta \ell_{Mi}) = \sum_{m=0}^3 (a_m \cdot \Delta \ell_{Mi}^m) \cdot p_{Mi} - \sum_{n=0}^4 (b_n \cdot \Delta \ell_{Mi}^n) \quad (7)$$

$$= \bar{F}_{Mi}(\Delta \ell_{Mi}) \cdot p_{Mi} - f_{Mi}(\Delta \ell_{Mi}).$$

III. NONLINEAR MODEL PREDICTIVE CONTROL (NMPC)

Predictive control represents a class of algorithms that are based on the prediction of the system states \mathbf{x} over a time span denoted prediction horizon T_P . Model predictive control implies that a process model is used for the prediction of the dynamic behaviour. An outline of NMPC is given by [5]. Based on the state space model and the measured state vector at time t_0 , the sequence of input variables according to a chosen cost function is calculated. After applying the first element of the input vector to the process, the optimization procedure is repeated at the following time instant with the prediction horizon moving forward: the moving horizon approach [6]. The main idea of the following algorithm consists of a minimization of the tracking error at the end of the prediction horizon T_P between the predicted state and the desired state resulting from trajectory planning [7], [8]. The minimization is achieved by repeated approximate numerical optimization in each time step, in the given case using the Newton-Raphson technique. The optimization is initialised in each time step with the optimization result of the preceding time step in form of the input vector. The NMPC-algorithm is based on the following nonlinear time-discrete state space representation

$$\mathbf{x}_{k+1} = \mathbf{f}(\mathbf{x}_k, \mathbf{u}_k), \quad \mathbf{y}_k = \mathbf{h}(\mathbf{x}_k, \mathbf{u}_k), \quad (8)$$

with the state vector $\mathbf{x}_k \in \mathcal{R}^n$, the control input $\mathbf{u}_k \in \mathcal{R}^m$, the output vector $\mathbf{y}_k \in \mathcal{R}^p$ and the initial vector $\mathbf{x}_0 \in \mathcal{R}^n$. The constant M specifies the prediction horizon T_P as a multiple of the sampling time t_s

$$T_P = M \cdot t_s. \quad (9)$$

The predicted input vector at time k becomes

$$\mathbf{u}_{k,M} = \left[\mathbf{u}_1^{(k)T}, \dots, \mathbf{u}_M^{(k)T} \right]^T, \quad (10)$$

with $\mathbf{u}_{k,M} \in \mathcal{R}^{m \cdot M}$. The predicted state vector at the end of the prediction horizon $\phi_M(\mathbf{x}_k, \mathbf{u}_{k,M})$ is obtained by repeated substitution of k by $k+1$ in the time-discrete state equation (8)

$$\begin{aligned} \mathbf{x}_{k+2} &= \mathbf{f}(\mathbf{x}_{k+1}, \mathbf{u}_{k+1}) = \mathbf{f}(\mathbf{f}(\mathbf{x}_k, \mathbf{u}_k), \mathbf{u}_{k+1}) \\ &\vdots \\ \mathbf{x}_{k+M} &= \underbrace{\mathbf{f}(\dots \mathbf{f}(\mathbf{x}_k, \mathbf{u}_k), \dots)}_M, \underbrace{\mathbf{u}_{k+M-1}}_M = \phi_M(\mathbf{x}_k, \mathbf{u}_{k,M}). \end{aligned} \quad (11)$$

The difference between $\phi_M(\mathbf{x}_k, \mathbf{u}_{k,M})$ and the desired state vector \mathbf{x}_d leads to the final control error

$$\mathbf{e}_{M,k} = \phi_M(\mathbf{x}_k, \mathbf{u}_{k,M}) - \mathbf{x}_d, \quad (12)$$

i.e., to the control error at the end of the prediction horizon. The quadratic cost function to be minimized follows as

$$J_{MPC} = \frac{1}{2} \cdot \mathbf{e}_{M,k}^T \mathbf{e}_{M,k}, \quad (13)$$

and, hence, the necessary condition for an extremum can be stated as

$$\frac{\partial J_{MPC}}{\partial \mathbf{e}_{M,k}} = \mathbf{e}_{M,k} \stackrel{!}{=} 0. \quad (14)$$

A Taylor-series expansion of (14) at $\mathbf{u}_{k,M}$ in the neighbourhood of the optimal solution leads to the following system of equations

$$\mathbf{0} = \mathbf{e}_{M,k} + \frac{\partial \phi_M}{\partial \mathbf{u}_{k,M}} \Delta \mathbf{u}_{k,M} + T.h.O. \quad (15)$$

The vector $\Delta \mathbf{u}_{k,M}$ represents the difference, which has to be added to the input vector $\mathbf{u}_{k,M}$ to obtain the optimal solution. The n equations (15) represent an under-determined set of equations with $m \cdot M$ unknowns having an infinite number of solutions. A unique solution for $\Delta \mathbf{u}_{k,M}$ can be determined by solving a L_2 -optimization problem with (15) as side condition, which leads to the Moore-Penrose pseudo inverse of $\frac{\partial \phi_M}{\partial \mathbf{u}_{k,M}}$ [1]

$$\Delta \mathbf{u}_{k,M} = - \left(\frac{\partial \phi_M}{\partial \mathbf{u}_{k,M}} \right)^+ \mathbf{e}_{M,k}. \quad (16)$$

One major advantage of predictive control is the possibility to easily account for input constraints, which are present in almost all control applications. To this end, the cost function can be extended with a corresponding term $h(\mathbf{u})$, see [1].

The overall NMPC-algorithm can be described as follows: Choice of the initial input vector $\mathbf{u}_{0,M}^{(d)}$ at time $k = 0$. For differential flat systems like the considered linear axis, the desired initial vector $\mathbf{u}_{0,M}^{(d)}$ can be calculated by evaluating an inverse system model (29) with the specified reference trajectory as well as a certain number of its time derivatives. Repetition of steps a) - c) at each sampling time $k \geq 0$:

- a) Calculation of an improved input vector $\mathbf{v}_{k,M}$ according to

$$\mathbf{v}_{k,M} = \mathbf{u}_{k,M} - \eta_k \left(\frac{\partial \phi_M}{\partial \mathbf{u}_{k,M}} \right)^+ \mathbf{e}_{M,k}. \quad (17)$$

The step width η_k can be determined with, e.g., the Armijo-rule [9].

- b) For the calculation of $\mathbf{u}_{k+1,M}$ the elements of the vector $\mathbf{v}_{k,M}$ have to be shifted by m elements and the desired input vector \mathbf{u}_d corresponding to the final state has to be inserted at the end

$$\mathbf{u}_{k+1,M} = \begin{bmatrix} \mathbf{0}_{(m(M-1) \times m)} & \mathbf{I}_{(m(M-1))} \\ \mathbf{0}_{m \times m} & \mathbf{0}_{(m \times m(M-1))} \end{bmatrix} \mathbf{v}_{k,M} + \begin{bmatrix} \mathbf{0}_{(m(M-1) \times m)} \\ \mathbf{I}_{(m)} \end{bmatrix} \mathbf{u}_d. \quad (18)$$

The desired input vector \mathbf{u}_d is given by the inverse dynamics (29).

- c) The first m elements of the improved input vector $\mathbf{v}_{k,M}$ are applied as control input at time k

$$\mathbf{u}(k) = \begin{bmatrix} \mathbf{I}_{(m)} & \mathbf{0}_{(m \times m(M-1))} \end{bmatrix} \mathbf{v}_{k,M}. \quad (19)$$

In the proposed algorithm only one iteration is performed per time step. A similar approach using several iteration steps is described in [10], [11].

A. Numerical Calculations

The analytical computation of the Jacobian $\frac{\partial \phi_M}{\partial \mathbf{u}_{k,M}}$ becomes increasingly complex for larger values of M . Therefore, a numerical approach is preferred taking advantage of the chain rule, $i = 0, \dots, M-1$

$$\frac{\partial \phi_M}{\partial \mathbf{u}_{i+1}^{(k)}} = \frac{\partial \phi_M}{\partial \mathbf{x}_{k+M-1}} \cdot \frac{\partial \mathbf{x}_{k+M-1}}{\partial \mathbf{x}_{k+M-2}} \dots \frac{\partial \mathbf{x}_{k+i+2}}{\partial \mathbf{x}_{k+i+1}} \cdot \frac{\partial \mathbf{x}_{k+i+1}}{\partial \mathbf{u}_{i+1}^{(k)}}. \quad (20)$$

Introducing the abbreviations

$$\mathbf{A}_i := \frac{\partial \mathbf{x}_{k+i+1}}{\partial \mathbf{x}_{k+i}} = \frac{\partial \mathbf{f}}{\partial \mathbf{x}} (\mathbf{x}_{k+i}, \mathbf{u}_{i+1}^{(k)}), \quad (21)$$

$$\mathbf{B}_i := \frac{\partial \mathbf{x}_{k+i+1}}{\partial \mathbf{u}_{i+1}^{(k)}} = \frac{\partial \mathbf{f}}{\partial \mathbf{u}} (\mathbf{x}_{k+i}, \mathbf{u}_{i+1}^{(k)}), \quad (22)$$

the Jacobian can be computed as follows

$$\frac{\partial \phi_M}{\partial \mathbf{u}_{k,M}} = [\mathbf{A}_{M-1} \mathbf{A}_{M-2} \dots \mathbf{A}_1 \mathbf{B}_0, \mathbf{A}_{M-1} \dots \mathbf{A}_2 \mathbf{B}_1, \dots, \mathbf{A}_{M-1} \mathbf{B}_{M-2}, \mathbf{B}_{M-1}]. \quad (23)$$

For the inversion of the matrix $\mathbf{S}(\phi_M, \mathbf{u}_{k,M}) = \frac{\partial \phi_M}{\partial \mathbf{u}_{k,M}} \left(\frac{\partial \phi_M}{\partial \mathbf{u}_{k,M}} \right)^T$, the Cholesky-decomposition has proved advantageous in terms of computational effort. It is supposed, that the matrix \mathbf{S} is symmetric and positive definite, thus the matrix $\frac{\partial \phi_M}{\partial \mathbf{u}_{k,M}}$ has full rank. However bad conditioned problems necessitate more expensive algorithms like the QR-factorization or the singular value decomposition [9].

B. Choice of the NMPC Design Parameters

The most important NMPC design parameter is the prediction horizon T_P , which is given as product of sampling time t_s and the constant value M as described by equation (9), see also fig. 5. Large values of T_P lead to a slow and smooth transient behaviour. For fast trajectory tracking, a smaller value T_P is desirable concerning a small tracking error. Very small values T_P , however, influence the stability negatively. The choice of the sampling time t_s is crucial as well: a small sampling time is necessary regarding discretisation error and stability; at the same time, however, the NMPC-algorithm has to be evaluated in real-time within the sampling interval. Furthermore, the smaller t_s , the larger becomes M for a given prediction horizon, which in turn increases the computational complexity of the optimization step. Consequently, a system-specific trade-off has to be made for the choice of M and t_s . This paper follows the moving horizon approach with a constant prediction horizon and, hence, a constant dimension $m \cdot M$ of the corresponding optimization problem in contrast to the shrinking horizon approach [10], [11].

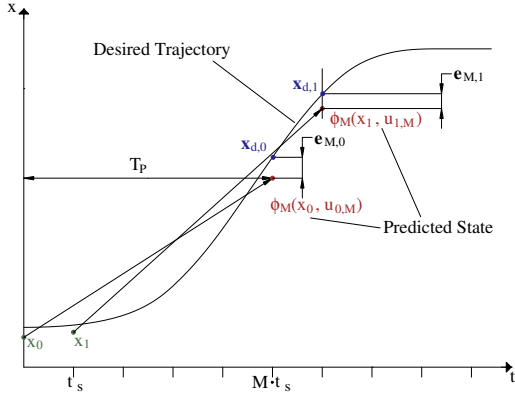


Fig. 5: Design parameters ($M = 5$)

IV. NMPC OF THE LINEAR AXIS

With the rocker angle φ , the angular velocity $\dot{\varphi}$ and the internal muscle pressures p_{Mi} as states and $\mathbf{u} = [u_{Ml}, u_{Mr}]^T$ as the input vector, the state space equation follows from equations (1) and (6). For discretisation the Euler approximation has been chosen. Thus, the computation effort remains relatively small in comparison to alternative methods, e.g. the Heun discretisation. Furthermore, no significant improvement was obtained for the given system with the Heun discretisation method because of the small sampling time $t_s = 2 \text{ ms}$. Only in the case of large sampling times, the increased computational effort by a sophisticated time discretisation method is advantageous. However, a small sampling time yields a smaller tracking error than a large sampling time, independent of the discretisation method.

Taking advantage of the differential flatness of the system [12], the desired input vector \mathbf{u}_d is calculated using desired values for the flat outputs \mathbf{y}_d and their time derivatives. Subsequent differentiations of the two flat outputs lead to

$$y_1 = \varphi, \quad \dot{y}_1 = \dot{\varphi}, \quad (24)$$

$$\ddot{y}_1 = \ddot{\varphi}(\varphi, \dot{\varphi}, p_{Ml}, p_{Mr}), \quad (25)$$

$$\ddot{\ddot{y}}_1 = \ddot{\ddot{\varphi}}(\varphi, \dot{\varphi}, \ddot{\varphi}, p_{Ml}, p_{Mr}, \dot{p}_{Ml}, \dot{p}_{Mr}), \quad (26)$$

$$y_2 = p_M = 0.5 \cdot (p_{Ml} + p_{Mr}), \quad (27)$$

$$\dot{y}_2 = \dot{p}_M = 0.5 \cdot (\dot{p}_{Ml} + \dot{p}_{Mr}). \quad (28)$$

These equations allow for calculating the desired input vector

$$\mathbf{u}_d = \begin{bmatrix} u_{ld}(y_1, \dot{y}_1, \ddot{y}_1, \ddot{\ddot{y}}_1, y_2, \dot{y}_2) \\ u_{rd}(y_1, \dot{y}_1, \ddot{y}_1, \ddot{\ddot{y}}_1, y_2, \dot{y}_2) \end{bmatrix}. \quad (29)$$

A. Reduced nonlinear disturbance observer

Disturbance behaviour and tracking accuracy in view of model uncertainties can be significantly improved by introducing a compensating control action provided by a nonlinear reduced-order disturbance observer. The observer design is based on the equation of motion, where the variable τ_U takes into account both the friction torques τ_{RS} and the remaining model uncertainties of the muscle force characteristics ΔF_M . The nonlinear disturbance observer is capable of counteracting impacts of changing carriage mass Δm_C as

well. The key idea for the observer design is to extend the state equation with an integrator as disturbance model

$$\dot{\mathbf{y}} = \mathbf{f}(\mathbf{y}, \tau_U, \mathbf{u}), \quad \dot{\tau}_U = 0, \quad (30)$$

where $\mathbf{y} = [\varphi, \dot{\varphi}]^T$ denotes the measurable state vector. The estimated disturbance torque is obtained from

$$\hat{\tau}_U = \mathbf{h}^T \cdot \mathbf{y} + z, \quad (31)$$

with the chosen observer gain vector $\mathbf{h}^T = [h_1 \quad h_1]$. The state equation for z is given by

$$\dot{z} = \Phi(\mathbf{y}, \hat{\tau}_U, \mathbf{u}). \quad (32)$$

The observer gain \mathbf{h} and the nonlinear function Φ have to be chosen, such that the steady-state observer error $e = \tau_U - \hat{\tau}_U$ converges to zero. Thus, the function Φ can be determined as follows

$$\dot{e} = 0 = \dot{\tau}_U - \mathbf{h}^T \cdot \mathbf{f}(\mathbf{y}, \tau_U, \mathbf{u}) - \Phi(\mathbf{y}, \tau_U - 0, \mathbf{u}). \quad (33)$$

In view of $\dot{\tau}_U = 0$, equation (33) yields

$$\Phi(\mathbf{y}, \tau_U - 0, \mathbf{u}) = -\mathbf{h}^T \cdot \mathbf{f}(\mathbf{y}, \tau_U, \mathbf{u}). \quad (34)$$

The linearised error dynamics \dot{e} has to be made asymptotically stable. Accordingly all eigenvalues of the Jacobian

$$\mathbf{J}_e = \frac{\partial \Phi(\mathbf{y}, \tau_U - e, \mathbf{u})}{\partial (\tau_U - e)} \quad (35)$$

must lie in the left complex half-plane. This can be achieved by proper choice of the observer gain h_1 . The stability of the observer control system have been investigated by thorough simulations.

B. Compensation of the valve characteristic

The nonlinear valve characteristic (VC) is compensated by pre-multiplying with its inverse valve characteristic (IVC) in each input channel. The valve characteristic has been identified by measurements. Here, the inverse valve characteristic depends both on the commanded mass flow and on the measured internal pressure and yields the appropriate input voltage u_{Vi} of the proportional valves.

V. EXPERIMENTAL RESULTS

The described NMPC scheme with the observer-based disturbance compensation has been implemented at the test rig of the University of Rostock. It is equipped with two pneumatic muscles DMSP-20 from FESTO AG. The internal pressures of the muscles are measured by piezo-resistive pressure sensors, while the carriage position is determined by a linear incremental encoder with an accuracy of $10 \mu\text{m}$. The desired trajectories for the carriage position, the internal pressures and their corresponding time derivatives are obtained from a trajectory planning module that provides synchronous time optimal trajectories. Here the desired z -position varies in an interval between -0.33 m and 0.33 m , see fig. 6. As can be seen, the maximum velocities are about 0.8 m/s . Hence, the utilised workspace and velocities are significantly larger than in [1] and [2] or in [13], where a mass is directly moved by a single

VI. CONCLUSION

In this paper, a nonlinear model predictive trajectory control is presented for a high-speed linear axis driven by pneumatic muscles. To increase both the workspace and the maximum velocity, the muscles are linked by a rocker to the carriage in comparison to a direct actuated solution. The modelling of this mechatronic system leads to a system of nonlinear differential equations of fourth order. For the nonlinear characteristics of the pneumatic muscles polynomials serve as good approximations. As the nonlinear valve characteristic is linearised by means of a pre-multiplication with its approximated inverse characteristic, the mass flow represents the new control input. One of the critical issues of NMPC design is the real-time solution of a optimization problem during each sampling interval. In the considered fast control application, the optimization problem was reduced to minimizing the predicted final state error at the end of the prediction horizon. In order to compensate remaining uncertainties in the muscle force as well as friction a nonlinear disturbance observer is adapted in the control structure. Experimental results show the good closed-loop performance with maximum position errors approx. 2 mm.

REFERENCES

- [1] H. Aschemann and D. Schindele, "Nonlinear model predictive control of a linear axis based on pneumatic muscles," *Proceedings of ICINCO 2007, Angers, France*, pp. 92–99, 2007.
- [2] H. Aschemann, D. Schindele, and E. Hofer, "Nonlinear optimal control of a mechatronic system with pneumatic muscle actuators," *CD-Proceedings of MMAR 2006, Miedzzydroje, Poland*, 2006.
- [3] P. Carbonell, Z. Jiang, and D. Repperger, "Comparative study for three nonlinear control strategies for a pneumatic muscle actuator," *Proceedings of NOLCOS 2001, Saint-Petersburg, Russia*, pp. 167–172, 2001.
- [4] M. Göttert, "Bahnregelung servopneumatischer Antriebe," *Berichte aus der Steuerungs- und Regelungstechnik (in German)*, Shaker Verlag, Aachen, 2004.
- [5] R. Findeisen and F. Allgöwer, "An introduction to nonlinear model predictive control," *Proceedings of 21st Benelux Meeting on Systems and Control, Veldhoven, Netherlands*, 2002.
- [6] M. Diehl, *Real-time optimization for large scale nonlinear processes*, *Fortschritt-Berichte VDI, Reihe 8, Nr. 920*. VDI Verlag, Düsseldorf, Germany, 2002.
- [7] J. W. F. Lizaralde and L. Hsu, "A new model predictive control strategy for affine nonlinear control systems," *Proceedings of the American Control Conference (ACC '99), San Diego*, pp. 4263–4267, 1999.
- [8] S. Jung and J. Wen, "Nonlinear model predictive control for the swing-up of a rotary inverted pendulum," *ASME J. of Dynamic Systems, Measurement and Control*, vol. 126, pp. 666–673, 2004.
- [9] J. Nocedal and S. Wright, *Numerical optimization, 2nd ed.* Springer, New York, 2006.
- [10] D. Weidemann, N. Scherm, and B. Heimann, "Discrete-time control by nonlinear online optimization on multiple shrinking horizons for underactuated manipulators," *Proceedings of the 15th CISM-IFToMM Symposium on Robot Design, Dynamics and Control, Montreal, Canada*, 2004.
- [11] D. Weidemann, N. Scherm, B. Heimann, and H. Abdellatif, "Nonlinear discrete-time control approaches for underactuated manipulators," *Proceedings of the 44th IEEE Conference on Decision and Control and the European Control Conference, Seville, Spain*, 2005.
- [12] H. Aschemann and E. P. Hofer, "Nonlinear trajectory control of a high-speed linear axis driven by pneumatic muscle actuators," *Proceedings of the 32nd Annual Conference of the IEEE 2006, Paris, France*, pp. 3857–3862, 2006.
- [13] A. Hildebrandt, O. Sawodny, R. Neumann, and A. Hartmann, "A flatness based design for tracking control of pneumatic muscle actuators," *Proceedings of ICARCV 2002, Singapore*, pp. 1156–1161, 2002.

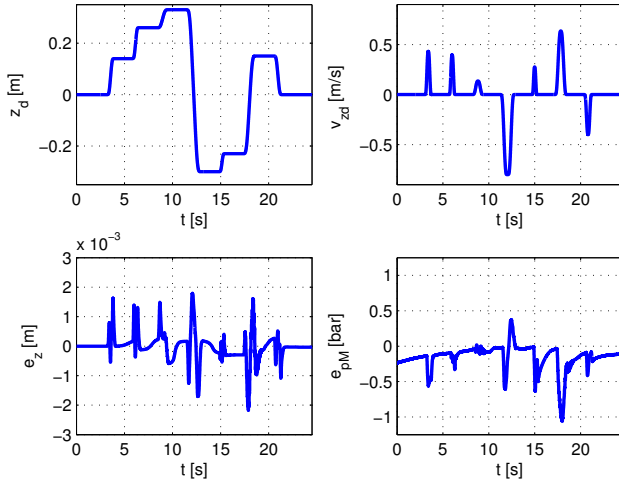


Fig. 6: Desired trajectories and according tracking errors for the carriage position and the mean pressure

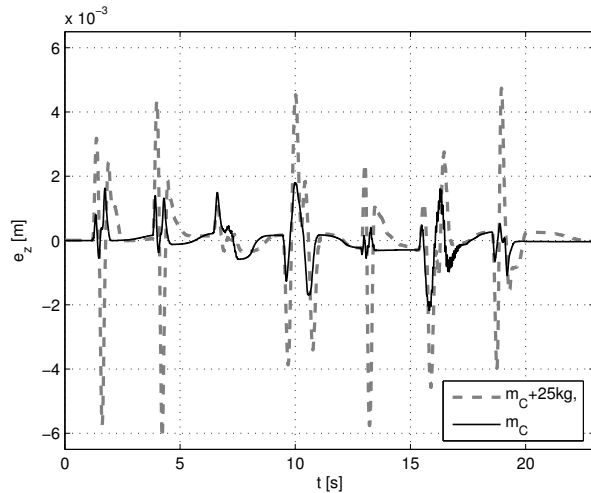


Fig. 7: Position error with changed mass of the carriage

pneumatic muscle. The mean pressure of the both muscles is kept constant on 4 bar during the whole experiment. The sampling time t_s was set to 2 ms to allow for evaluating the NMPC-algorithm in real-time and, moreover, to constrain the discretisation error. In the lower part of fig. 6, the obtained results are depicted for a prediction horizon $T_P = 150$ ms, i.e. $M = 75$. The maximum tracking error for the carriage position during the acceleration and deceleration intervals is approx. 2 mm, the maximum steady-state error about 0.3 mm. The tracking error of the mean pressure during the movements is below 1.1 bar, whereas the steady-state pressure error is smaller than 0.1 bar. In fig. 7 the robustness of the controlled system regarding a changing mass of the carriage is demonstrated. An increase in the carriage mass $m_C = 18$ kg about 25 kg leads to a maximum position error of 6 mm, the steady state error is still smaller than 0.3 mm.